Excited state wavepacket dynamics in NO_2 probed by strong-field ionization

Ruaridh Forbes,[1,2,3] Andrey E. Boguslavskiy,[2,3,4] Iain Wilkinson,[2,5]
Jonathan G. Underwood,[1] and Albert Stolow[2,3,4,a)]
[1]*Department of Physics and Astronomy, University College London, Gower Street, London WC1E 6BT, United Kingdom*
[2]*National Research Council of Canada, 100 Sussex Drive, Ottawa, Ontario K1A 0R6, Canada*
[3]*Department of Physics, University of Ottawa, 150 Louis Pasteur, Ottawa, Ontario K1N 6N5, Canada*
[4]*Department of Chemistry, University of Ottawa, 10 Marie Curie, Ottawa, Ontario K1N 6N5, Canada*
[5]*Methoden der Materialentwicklung, Helmholtz-Zentrum Berlin für Materialien und Energie GmbH, Hahn-Meitner-Platz 1, 14109 Berlin, Germany*

(Received 19 April 2017; accepted 17 July 2017; published online 4 August 2017)

We present an experimental femtosecond time-resolved study of the 399 nm excited state dynamics of nitrogen dioxide using channel-resolved above threshold ionization (CRATI) as the probe process. This method relies on photoelectron-photoion coincidence and covariance to correlate the strong-field photoelectron spectrum with ionic fragments, which label the channel. In all ionization channels observed, we report apparent oscillations in the ion and photoelectron yields as a function of pump-probe delay. Further, we observe the presence of a persistent, time-invariant above threshold ionization comb in the photoelectron spectra associated with most ionization channels at long time delays. These observations are interpreted in terms of single-pump-photon excitation to the first excited electronic $\tilde{X}\ ^2A_1$ state and multi-pump-photon excitations to higher-lying states. The short time delay (<100 fs) dynamics in the fragment channels show multi-photon pump signatures of higher-lying neutral state dynamics, in data sets recorded with higher pump intensities. As expected for pumping NO_2 at 399 nm, non-adiabatic coupling was seen to rapidly re-populate the ground state following excitation to the first excited electronic state, within 200 fs. Subsequent intramolecular vibrational energy redistribution results in the spreading of the ground state vibrational wavepacket into the asymmetric stretch coordinate, allowing the wavepacket to explore nuclear geometries in the asymptotic region of the ground state potential energy surface. Signatures of the vibrationally "hot" ground state wavepacket were observed in the CRATI spectra at longer time delays. This study highlights the complex and sometimes competing phenomena that can arise in strong-field ionization probing of excited state molecular dynamics. [http://dx.doi.org/10.1063/1.4996461]

I. INTRODUCTION

The uses of strong-field ionization (SFI) and high-harmonic generation (HHG) as probe techniques in the study of molecular electronic dynamics, with potentially subfemtosecond time resolution, has received considerable attention.[1–7] For example, UV pump-HHG probe spectroscopy was used for studies of molecular wavepacket dynamics in the molecules N_2O_4,[4] Br_2,[6] NO_2,[8–10] CH_3I, and CF_3I.[11] In the interpretation of HHG experiments, extensive use was made of the three-step model,[12,13] where an electron is ionized by a strong laser field and subsequently undergoes acceleration in this field before (if it has the right phase) recolliding and recombining with the parent ion core, emitting a burst of extreme ultraviolet (XUV) light. The majority of these studies have been concerned with atoms or diatomic molecules, where semi-analytical SFI theories provide guides to the interpretation of experimental results.[12,13] Here we present a pump-SFI probe study of excited state wavepacket dynamics in the molecule NO_2.

The SFI processes of above threshold ionization (ATI) and HHG are both subcycle phenomena and are closely related. ATI, within the narrative of the three-step model, can be considered a measure of the first (ionization) step in HHG.[12,13] For both ATI and HHG, it is the repetition of the sub-cycle SFI phenomenon at every laser cycle that leads to the observed periodicity in the photoelectron (ATI) or XUV (HHG) spectra.[14]

There are both experimental and theoretical challenges in the use of SFI probes of polyatomic wavepacket dynamics, particularly in electronically excited states where both geometry and electronic structure will evolve significantly with time. This means that, within the narrative of the three-step model, both the first step—involving SFI rates—and the third step—involving recombination dipole matrix elements—will vary as the wavepacket evolves. It will therefore be important, in interpreting the results of strong-field experiments on molecular dynamics, to understand the relative roles of the SFI rate and recombination dipoles as a function of dynamical evolution. Due to the deep relationship between ATI and HHG, the former can be used as a measure of the SFI rate as a function of time as it contributes to HHG experiments.

a)Albert.Stolow@nrc-cnrc.gc.ca

A major problem in the analysis of experimental results when using strong laser fields is the possibility of accessing multiple electronic continua (i.e., ionization into ground and electronically excited states of the ion), which are known to play a role in even simple molecules such as N_2,[15] HCl,[16] CO_2,[5,17] N_2O_4,[4,18] SF_6,[19] and acetylene.[20] The extent to which multielectron dynamics play a role varies between molecules, but it can potentially be assessed experimentally by examining the ratios of channel-resolved ionization yields to different final ionic states. Typically, the excited ionic states of polyatomic molecules undergo rapid radiationless transitions, which often results in fragmentation.[21] Monitoring the degree and channel of fragmentation, through methods such as mass spectrometry following SFI, therefore also allows assessment of the role of multielectron dynamics. However, typical femtosecond laser pulses comprise multiple optical cycles. Hence this means that a bound electron within an ionized molecule can be further excited within the same laser pulse. This post-ionization excitation therefore presents another route to SFI-induced molecular ion fragmentation. Finally, even within a single laser field cycle, non-resonant, non-adiabatic excitations to cation excited states may occur. This field-driven, inter-channel coupling process has been termed non-adiabatic multielectron (NME) ionization.[22,23] The observation of ionic fragmentation alone, therefore, does not suffice to disentangle direct ionization to excited states of the ion (relevant to HHG) from post-ionization excitation from the ionic ground state.

We previously developed an ATI probe technique that is resolved with respect to the SFI electronic continuum channel, a method we termed Channel-Resolved ATI (CRATI).[1,2] The method utilizes the fact that if ionization correlates directly to a cation excited state, then the ATI photoelectron comb may be shifted energetically compared to that for ionization correlating to the cation ground state, due to the difference in ionization potential for the respective ionization channels. Conversely, if excited ionic states were populated post-ionization, then the ATI photoelectron departed before subsequent excitation occurs. This results in the ATI photoelectron comb being the same as that of the state prepared by direct ionization (i.e., post-ionization excitation cannot influence the departed continuum electron). Here we apply a Time-Resolved CRATI (TRCRATI) method in a pump-probe configuration to the study of excited state non-adiabatic wavepacket dynamics in the canonical system NO_2, pumped at 399 nm.

The NO_2 molecule is an exemplary system with which to study strong-field probing of photoexcited polyatomic molecules due to the presence of non-adiabatic couplings between electronic states, intramolecular vibrational energy redistribution (IVR), and neutral dissociation pathways. The literature associated with this system is extensive in both the frequency[24–32] and time domains[8–10,33–39] and hence adds to the suitability of NO_2 as an important system for studying the nature of pump-SFI probe spectroscopies in polyatomics. The photodynamics of NO_2 have been reviewed and summarised by Wilkinson and Whitaker.[40]

In our experimental study, we focus on the dynamics close to the first dissociation limit at 3.1155 eV.[40] Single-photon vertical photoexcitation at wavelengths around the first dissociation limit transfers population from the $\tilde{X}\ ^2A_1$ state to the $\tilde{A}\ ^2B_2$ state. Initially, the wavepacket motion on the excited state is quasi-one-dimensional along the bending coordinate and moves rapidly towards a conical intersection between the $\tilde{A}\ ^2B_2$ and $\tilde{X}\ ^2A_1$ states. The wavepacket can either cross the intersection diabatically or adiabatically.[41,42] The diabatic wavepacket is expected to make several passes of the intersection but with significant non-adiabatic population transfer to the ground state within 50 fs and almost complete transfer to the ground state within approximately 200 fs.[41] In addition, within a few hundred femtoseconds, IVR results in the wavepacket spreading into the asymmetric stretch coordinate and, for molecules with an internal energy above 3.1155 eV, neutral dissociation producing $NO(X^2\Pi)$ and $O(^3P)$ via unimolecular decay on a picosecond time scale.[43]

Numerous femtosecond time-resolved studies have been carried out to investigate the dynamics originating from the $\tilde{A}\ ^2B_2$ state, employing a range of techniques such as two-colour fluorescence depletion,[33] mass spectrometry,[37] and velocity map imaging (VMI) of photoions and photoelectrons,[35,39] coincidence imaging studies,[36,38] and novel high-harmonic probes.[8–10] Recently a series of femtosecond time-resolved imaging experiments employing pulses at 400 nm and 266 nm have investigated photofragmentation dynamics in NO_2. These experimental studies reported time-dependent oscillations in the NO^+ fragment and slow (near 0 eV) photoelectron yields with periods in the range of 500-850 fs.[34,35,38,39] A series of differing interpretations have been suggested as to the origin of the observed modulations, including: the energy level spacing between coupled levels in the $\tilde{A}\ ^2B_2$ and $\tilde{X}\ ^2A_1$ states close to their conical intersection;[34] wavepacket motion along a "soft coordinate" with a corresponding energy level spacing of 40 cm^{-1}, with the motion potentially linked to a free rotation of an oxygen atom around an NO core at large NO–O bond lengths[35] (roaming atom mechanism[44]); motion in the asymmetric stretch coordinate; and resonances between symmetric stretch and bend vibrations at energies close to the $NO(X^2\Pi)$ and $O(^3P)$ dissociation threshold.[45]

Recently, time-resolved HHG studies reported a small number of oscillations in high harmonic signal with a period on the order of 100 fs, which was assigned to $\tilde{A}\ ^2B_2/\tilde{X}\ ^2A_1$ vibronic coupling[8] due to its similar appearance to the theoretical predictions.[10,41] In contrast to both the imaging and HHG studies, 200 fs oscillations were observed in time-resolved mass spectrometry studies,[37] which have again been tentatively assigned to conical intersection dynamics. However, recent coincidence imaging studies employing pulses at 400 nm and 266 nm have identified a number of different competing multiphoton pump laser channels leading to the formation of NO_2^+ or NO^+ cations and corresponding photoelectrons.[36,38] The participation of multiphoton pump laser channels may equally occur but be obfuscated in less differential (i.e., not channel-specific) measurements such as time-resolved mass spectrometry or high harmonic spectroscopy. This therefore may effect the interpretation of the previous experimental results. With this in mind and the ambiguity in the interpretation of the

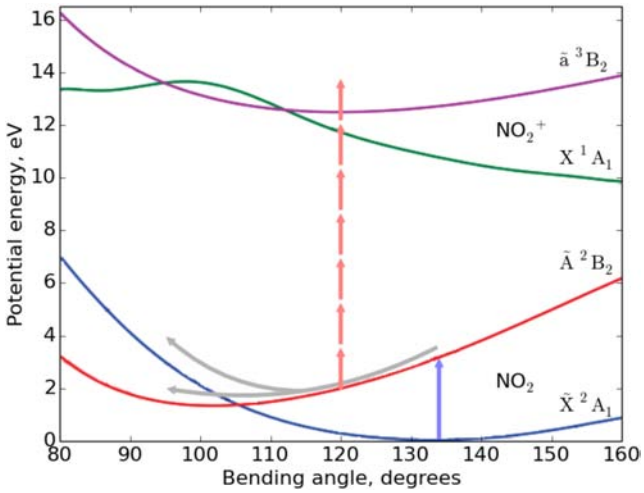

FIG. 1. Potential energy surfaces as a function of ONO bending angle for the important electronic states of NO_2 and NO_2^+ involved in single-photon excitation and subsequent strong-field probing at 798 nm (red arrows). Photoexcitation at 399 nm (blue arrow) prepares a vibrational wavepacket on the $\tilde{A}\ ^2B_2$ state, which subsequently transfers population back to the $\tilde{X}\ ^2A_1$ state via a conical intersection. Adapted with permission from Arasaki *et al.*, J. Chem. Phys. **132**, 124307 (2010). Copyright 2010 AIP Publishing LLC.

oscillations observed via different probe schemes, we revisit here the excited state dynamics of NO_2. In this present study, we utilize 399 nm pump and 798 nm strong-field probe pulses in conjunction with photoelectron photoion coincidence (PEPICO) spectroscopy to investigate the dynamics following excitation to the $\tilde{A}\ ^2B_2$ state and to assess contributions of multiphoton pump excitation channels in the observed dynamics (see Fig. 1).

This manuscript is structured as follows. In Sec. II, a description of the experimental setup is given, in Sec. III the data analysis tools used in the interpretation of the PEPICO spectra are presented, and in Sec. IV experimental results are shown. In Sec. V, we interpret the experimental results in terms of single and multiphoton pump laser dynamics and, finally, our conclusions are summarised in Sec. VI.

II. EXPERIMENTAL SETUP

The laser system employed for these experiments (Legend Elite Duo, Coherent, Inc.) delivered 35 fs pulses at 798 nm with a pulse energy of 4 mJ at a repetition rate of 1 kHz. A 0.5 mJ component of this beam was used for these experiments and attenuation was provided by a half waveplate and a set of thin film polarizers. The beam was passed through an 85:15 beamsplitter to provide the pump and probe beams, respectively. The reflected 85% was frequency doubled using a 200 μm Beta Barium Borate (β-BaB_2O_4), BBO, crystal cut at 29.2° to provide 399 nm pulses with an estimated pulse duration of 40 fs. A half waveplate at 798 nm was placed before the BBO crystal in order to provide independent attenuation of the pump pulse power. Dichroic mirrors with high reflectivity at 399 nm and high transmission at 798 nm were used for separating the fundamental and second harmonic and also for recombining the pump and probe beams in a collinear geometry. The collinear beams were focused into the spectrometer using an $f = 0.5$ m spherical mirror. The Rayleigh range of each beam at the foci was estimated to be 12 mm and 6 mm and the approximate Gaussian beam radii at the foci was 280 μm and 140 μm at 798 nm and 399 nm, respectively. The time delay between the pump and probe beams was varied using a computer controlled delay stage (Newport XML210) and a set of retroflector mirrors. The zero pump-probe delay was determined *in-situ* by examining the non-resonant ionization signal of background and co-expanded gases in the spectrometer (H_2O and O_2) and fitting a Gaussian function to the TRCRATI spectra for the associated parent ion channels. The average temporal cross-correlation was determined to be 55 fs (FWHM). Linearly polarized laser pulses were employed throughout the measurements, with the relative polarization between the two beams being controlled and varied using a halfwave plate at 399 nm mounted in a computer controlled rotation stage placed in the pump beamline prior to pump-probe recombination. Throughout the experiments, the polarization of the 798 nm probe was fixed to remain parallel to the spectrometer-time-of-flight (ToF) axis, in order to maintain constant photoelectron detection efficiency.

The PEPICO/CRATI spectrometer used to carry out these experiments was described previously in Refs. 1, 2, and 46. A 1.5% mixture of NO_2 (Praxair Canada, Inc., 99.5%) seeded in He (BOC GAZ, 5N purity) was continuously expanded through a 50 μm pinhole into a source chamber held at a pressure of around 3×10^{-6} Torr (molecular beam on). Additionally, 3% O_2 (Praxair Canada, Inc., 5N purity) was added to the gas mixture in order to displace the equilibrium between NO and NO_2 towards NO_2. The molecular beam was skimmed to a diameter of approximately 1 mm before entering a separate detection chamber, typically held at a base pressure of 1×10^{-8} Torr during the molecular beam experiment. The laser intersected the molecular beam at 90° at a distance of 600 mm from the second skimmer. By design, the long Rayleigh range of the laser foci ensures a constant axial intensity in the laser ionization volume, thus minimizing the effects of volume spatial intensity averaging. For all experiments reported here, the expansion was created using a nozzle held at 350 K to ensure an NO_2/N_2O_4 equilibrium of 99.8% in favour of the monomer. Additionally, it should be noted that N_2O_4 has an extremely low single-photon excitation probability at 399 nm.[47] Photoelectrons were extracted from the laser-molecular beam interaction region by a large bore (20 mm ID) icosapole (20-pole) permanent magnet, magnetic bottle spectrometer.[48] The spectrometer is designed to ensure efficient collection of photoelectrons, >75% (i.e., magnetic mirror mode), by placing the interaction region on the negative slope of the axial magnetic field intensity, which allows the trajectories of a subset of electrons emitted in the opposite direction to the electron ToF region to be reversed. The magnetic bottle had an energy resolution of $\Delta E = 160$ meV at 1 eV and photoelectrons were collected up to an energy of 15 eV. Coincident ion detection was achieved by means of a coaxial pulsed Wiley-McLaren ToF mass spectrometer.[49] The ion ToF was operated under Wiley-McLaren space and energy focussing conditions to maximize mass resolution. The ToF axis of the spectrometer was oriented perpendicular to both the laser and molecular beam propagation directions and detection of single

ions and electrons was performed using two sets of triple-stack microchannel plate (MCP) detectors. The resulting ion and electron signals were amplified (Philips Scientific 300 MHz Bipolar Amplifier 6950), passed through a constant fraction discriminator (Philips Scientific 300 MHz Discriminator 6904), and their arrival time recorded using a multichannel scaler card (FAST Comtec GmbH P788).

The total TRCRATI spectra were generated by scanning the pump-probe delay over a range between −250 and +10 000 fs, with variable step sizes. Pump-probe delay scans were performed with high-temporal resolution (step size 10-20 fs) between −250 and +500 fs only. At each time delay, pump-probe and time-independent probe-alone signals were recorded for 5000 and 1000 laser shots, respectively. Additionally, time-independent pump-alone signals were recorded for 1000 laser shots in higher intensity experiments where pump-alone counts were observed. However, negligible signals were typically observed in the pump-alone case. The TRCRATI spectra were recorded for two linear polarization geometries: (i) pump and probe polarization vectors set parallel to the ToF axis of the spectrometer, referred to as the parallel geometry; and (ii) with the pump set perpendicularly to the probe polarization and the ToF axis, referred to as the perpendicular geometry. The polarization between the pump and probe pulses was rotated between the two geometries every consecutive time-delay scan. The pump-probe delay range was swept through 20-30 times, depending on the signal strength, for each of the polarization geometries. Spectra of the pump and probe pulses were recorded using a spectrometer (USB4000 Ocean Optics, Inc.) before and after each of the experimental runs.

III. DATA ANALYSIS

The photoelectron and photoion ToF signals were correlated using covariance mapping, thus correlating a photoelectron signal with specific ion channels. The advantage of using the covariance mapping method, introduced by Frasinski and co-workers,[50,51] compared to true coincidence is that data can be collected at higher acquisition rates, with greater than an order of magnitude increase in event rate being possible. The covariance between an ion ToF, t_i (corresponding to mass, m_i), and a photoelectron ToF, t_e (corresponding to kinetic energy, E_e), is given by

$$\mathrm{cov}[I(t_i), E(t_e)] = \overline{I(t_i)E(t_e)} - \overline{I(t_i)} \cdot \overline{E(t_e)}, \qquad (1)$$

where the ion-electron covariance is evaluated for each laser shot and the average is evaluated over all laser shots. For a given laser shot, $I(t_i)$ and $E(t_e)$ are the number of ions at a specific mass and photoelectrons at a specific kinetic energy, respectively. The total TRCRATI spectrum was then constructed by performing the above covariance analysis at each point in the pump-probe time delay range. In all presented data, the covariant pump-alone (where required) and probe-alone signals were subtracted from the pump-probe signal.

The recording of the two orthogonal pump and probe polarization geometries permits the linear dichroism (LD) to be extracted. The LD provides a measure of the anisotropy of photoionization between the two polarization geometries and assesses any dependence on the alignment created in the excited state by the pump pulse. We express the time-dependent linear dichroism (TDLD) as

$$\mathrm{LD}(\parallel, \perp, E, t) = \frac{I(\parallel, E, t) - I(\perp, E, t)}{\max(I(\parallel, E, t) - I(\perp, E, t))}, \qquad (2)$$

where $\parallel$ and $\perp$ refer to the parallel and perpendicular polarization geometries, respectively, and I refers to the intensity of the signal. Equation (2) has been normalized to the maximum value of the difference between the parallel and perpendicular signals. In the case of the TDLD associated with the mass spectrum, we note that the kinetic energy dependence can be neglected due to the mass spectrum (in our implementation) being a kinetic energy integrated observable.

IV. RESULTS

In order to study the dynamics of photoexcited NO_2 molecules, we recorded TRCRATI spectra at three different pump intensities and, at each pump intensity, three different probe intensities. The pump intensities used were estimated to be 0.2×10^{13} W cm^{-2}, 0.8×10^{13} W cm^{-2}, and 3.6×10^{13} W cm^{-2}. The estimated probe intensities used were 3.6×10^{13} W cm^{-2}, 4.3×10^{13} W cm^{-2}, and 5.5×10^{13} W cm^{-2}. From each of these experiments, TRCRATI spectra were recorded for the NO_2^+, NO^+, and O^+ channels. Initially, we consider experiments with the pump and probe intensities set at 0.8×10^{13} W cm^{-2} and 3.6×10^{13} W cm^{-2}, respectively. Example mass spectra are shown for the parallel polarization geometry for several time delays (0 fs, 300 fs, and 1000 fs) in Fig. 2. Under the conditions employed in this study, the NO^+ fragment yield varied between 0.25 and 8 times that of NO_2^+ depending on the pump and probe intensities, as well as on the

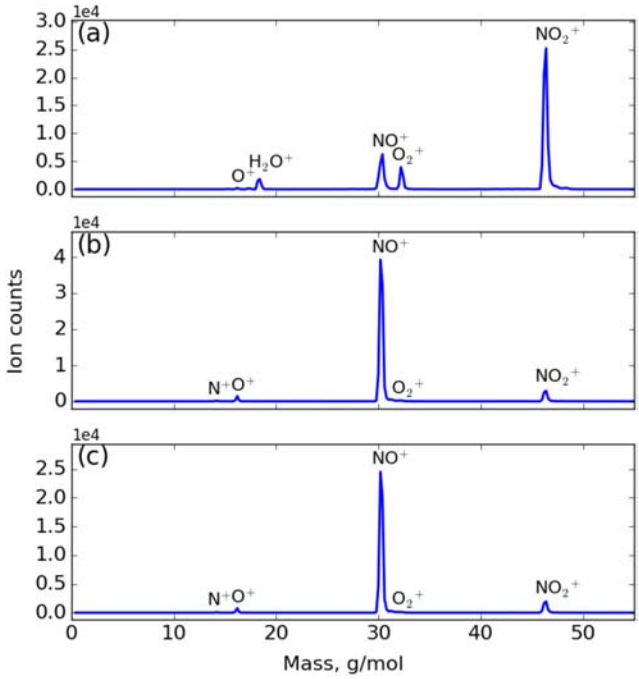

FIG. 2. Mass spectra recorded in the parallel polarization geometry at (a) 0 fs, (b) 300 fs, and (c) 1000 fs time delay. The spectra were recorded with an estimated pump and probe intensity of 0.8×10^{13} W cm^{-2} and 3.6×10^{13} W cm^{-2}, respectively.

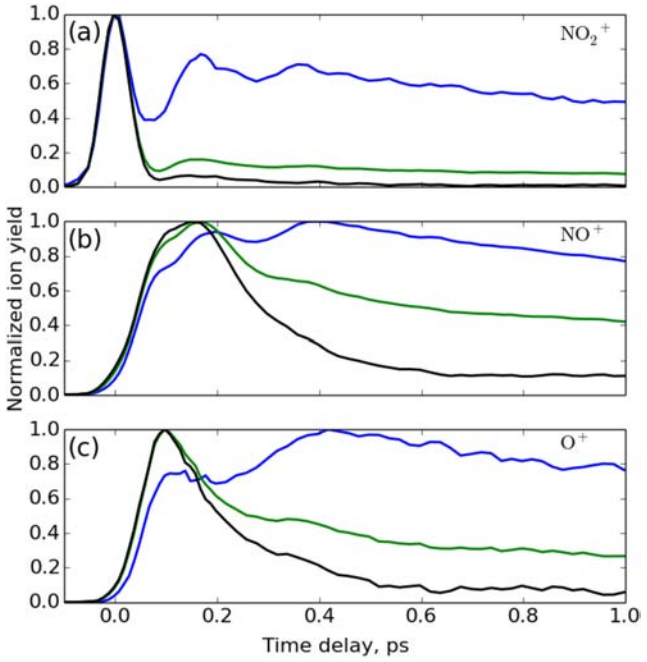

FIG. 3. Time-resolved ion-yield spectra (TRIYS) recorded for NO_2^+ (a), NO^+ (b), and O^+ (c) at an estimated pump and probe intensity of 0.8×10^{13} W cm^{-2} and 3.6×10^{13} W cm^{-2}, respectively. Data are presented for both the perpendicular (blue) and parallel (green) polarization geometries as well as the TDLD signal (black).

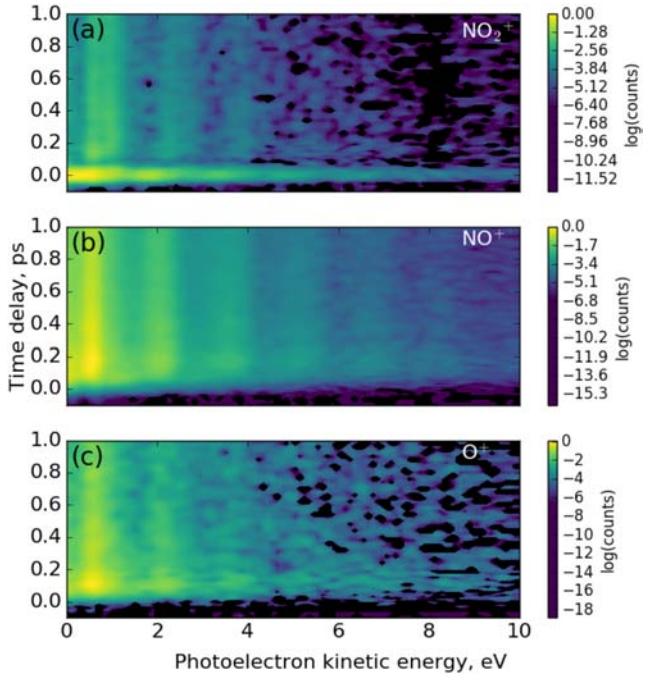

FIG. 4. TRCRATI spectra for the NO_2^+ (a), NO^+ (b), and O^+ (c) ion channels. The spectra were recorded in the parallel polarization geometry with an estimated pump and probe intensity of 0.8×10^{13} W cm^{-2} and 3.6×10^{13} W cm^{-2}, respectively. We note that the appearance of empty data bins in the spectra originates from the probe-alone background subtraction. In cases where a negative counts value was generated, the data point in question was not displayed during plotting; negative counts would result in errors in the log scale.

polarization geometry. In contrast, the signal in the O^+ channel always remained smaller, typically 20% of the parent ion channel out to the maximum measured time delay.

In Fig. 3 we show Time-resolved ion-yield spectra (TRIYS) for NO_2^+ [panel (a)], NO^+ [panel (b)], and O^+ [panel (c)] for the perpendicular and parallel polarization geometries, as well as the TDLD. All TRIYS exhibited time-dependent modulations and have non-monotonic behaviour. At the temporal overlap of the pump and probe fields (time zero), a sharp non-resonant signal is observed in the NO_2^+ signal. Outside this region, a series of rising signals were observed in all channels, initially peaking at approximately 110 fs in O^+ and at 180 fs in both NO^+ and NO_2^+. Additionally, the NO^+ signal exhibited a "shoulder" at 80 fs time delay. All three channels exhibited a subsequent peak in their signals at 380-400 fs, which itself then decays on a picosecond time scale. The TDLD signals (black) display behaviour different from the ion yields in all channels within the first 500 fs but decaying towards zero outside this region (see Fig. 3).

The TRCRATI spectra for the NO_2^+ [panel (a)], NO^+ [panel (b)], and O^+ [panel (c)] ion channels are presented in Fig. 4 for the parallel polarization geometry. Outside the temporal overlap of the two pulses, a sharp ATI comb is observed in the TRCRATI spectra for all three channels, which persists out to the maximum measured pump-probe delay of 10 ps. A number of interesting observations can be drawn from the comparison of TRCRATI spectra associated with different cations. Firstly, the NO_2 correlated spectra exhibit two distinct ATI combs outside the cross-correlation region, indicating that the stable parent ion can be formed via multiple strong-field ionization channels. The lower energy ATI comb ($0.5 + n\hbar\omega$ eV) is also present in both the NO^+ and O^+ fragment correlated spectra, suggesting that sequential processes are participating in the ionization dynamics, whereas the higher energy ATI comb ($0.9 + n\hbar\omega$ eV) appears only in the NO_2^+ channel. Secondly, temporal modulations were observed in the ATI comb intensity but not in the comb peak position, with the signal modulations exhibiting the same temporal behaviour as the photoion signal (Fig. 3). Finally, a number of less intense short lived features at around 1 eV were observed in the fragment channels and have a limited progression at higher photoelectron kinetic energy. The onset of the short lived ATI comb matches the features observed at 80 fs in the NO^+ and O^+ TRIYS [see Figs. 3(b) and 3(c)].

In order to investigate the possible origins of these differences and the temporal modulations observed in the photoelectron and ion yields, we systematically varied the intensities of the pump and probe pulses. These studies allowed us to determine the possible contributions of multi-photon excitations to higher-lying neutral states in the pump step as well as additional ionization channels accessed during strong-field probing.

In Fig. 5, we show the TRIYS for NO_2^+ [panel (a)], NO^+ [panel (b)], and O^+ [panel (c)] as a function of pump pulse intensity. The dynamics in the NO_2^+ parent ion channel shows very little dependence on the pump intensity, apart from the expected increase in the non-resonant signal at zero time delay. Conversely, the fragment channels show the opposite behaviour, at short time delays, with features that emerge at higher pump intensities. This pump intensity dependence indicates the accessing of higher-lying electronically excited states in neutral NO_2, through multiphoton excitations in the

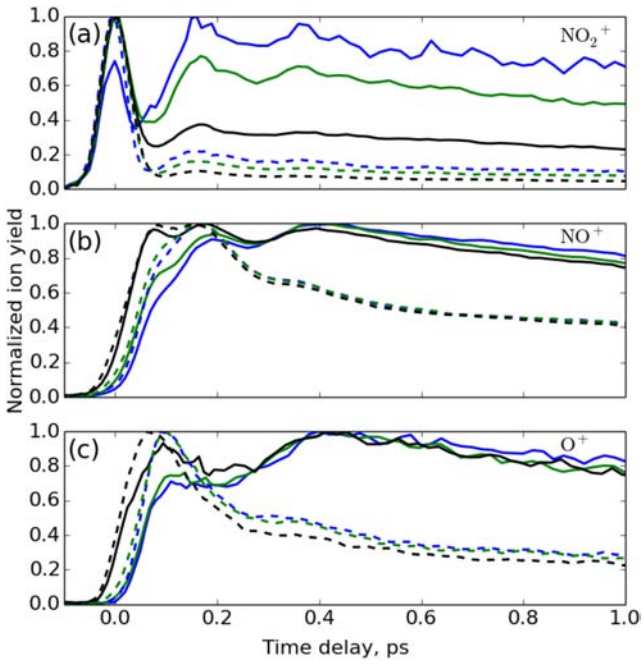

FIG. 5. Pump laser intensity dependence of the time-resolved ion-yield spectra recorded for NO_2^+ (a), NO^+ (b), and O^+ (c) in the parallel (dashed lines) and perpendicular (solid lines) polarization geometries. The data were collected with three different pump intensities, 0.2×10^{13} W cm^{-2} (blue), 0.8×10^{13} W cm^{-2} (green), and 3.7×10^{13} W cm^{-2} (black) at a constant probe laser intensity of approximately 3.6×10^{13} W cm^{-2}.

pump step. Additionally, the TDLD (not shown) highlights that the features observed at higher pump intensities in the NO^+ and O^+ channels exhibit a dependence on the relative polarization geometry, with enhancement in the signal observed in the parallel geometry.

To further examine the origins of the pump-power-dependent features, we present TRCRATI spectra, again as a function of pump intensity (Fig. 6) for the parallel polarization geometry. It can be clearly seen that, at time delays <100 fs, the modulation structure of the ATI combs becomes significantly less pronounced at higher pump intensities [Figs. 6(c) and 6(d)]. Furthermore, in the correlated photoelectron spectra for both fragments, the less intense short-lived spectral features at around 1 eV (and higher ATI order photoelectron peaks) become more pronounced at higher pump intensities [Figs. 6(e) and 6(f) red dashed lines].

Finally, we turn our attention to the effect of the probe laser intensity on the experimental observables. The TRIYS (not shown) for NO_2^+, NO^+, and O^+ were relatively unchanged for the three probe intensities considered within this work, apart from an overall increase in the non-resonant signal observed in the NO_2^+ at higher probe intensities. In Fig. 7, we show the TRCRATI spectra for all three channels, in the parallel polarization geometry, for the lowest (3.6×10^{13} W cm^{-2}) and highest (5.5×10^{13} W cm^{-2}) 798 nm probe intensities studied here. In the fragment channels, it is evident that the modulation structure of the ATI combs diminishes in the higher probe intensity data set [Figs. 7(d)–7(f)]. Analysis of the ground state, probe-alone, CRATI spectra (not shown) highlighted that some broadening of the ATI comb was observed at higher probe laser intensities. This can be linked to intensity averaging originating from an increased interaction volume of the probe laser with the molecular beam. It should be noted that the participation of additional ionization channels, due to the higher intensity probe ionizing from broader regions of coordinate space and/or accessing higher-lying ionization continua, may also play a role. Disentangling the relative

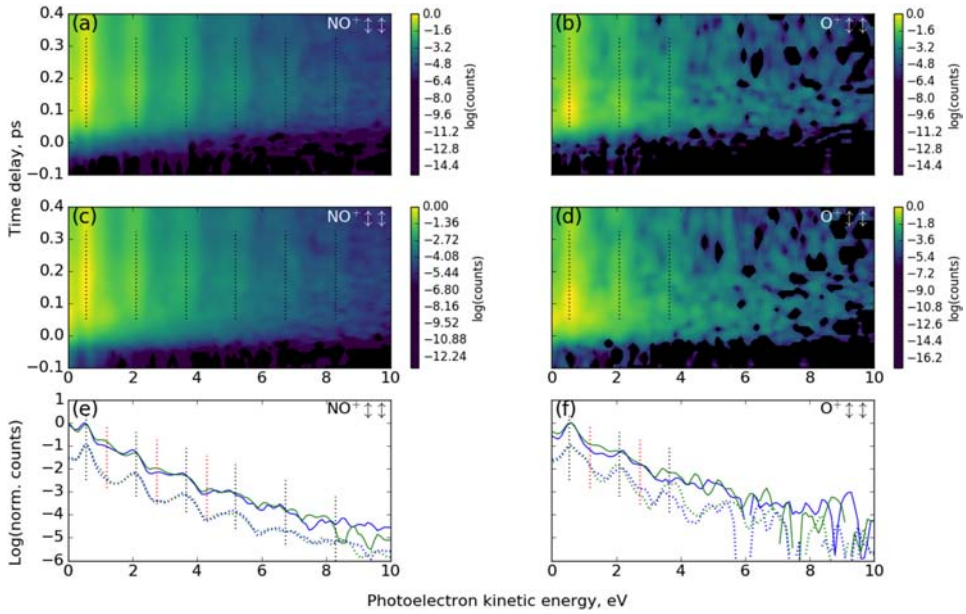

FIG. 6. TRCRATI spectra associated with NO^+ (left column) and O^+ (right column) channels at two pump laser intensities: Panels (a) and (b) $I_{pump} = 0.2 \times 10^{13}$ W cm^{-2}; panels (c) and (d) $I_{pump} = 3.7 \times 10^{13}$ W cm^{-2}. The spectra were recorded with a constant probe intensity of 3.6×10^{13} W cm^{-2}, and data are presented for the parallel polarization geometry. Panels (e) and (f) show line-outs of the TRCRATI spectra at $\Delta t = 80$ (solid line) and 180 fs (dashed line) for the two pump intensities, 0.2×10^{13} W cm^{-2} (blue) and 3.7×10^{13} W cm^{-2} (green). The dotted black lines in all panels indicate the main ATI comb observed. In panel (e), the red dotted line indicates a second ATI comb that appears at the 80 fs time delay (solid line), most prominently for the higher intensity pump (green). This transient, high pump intensity ATI comb, which vanishes at longer time delays, is seen only weakly in panel (f), due to the low count rate in the O^+ channel.

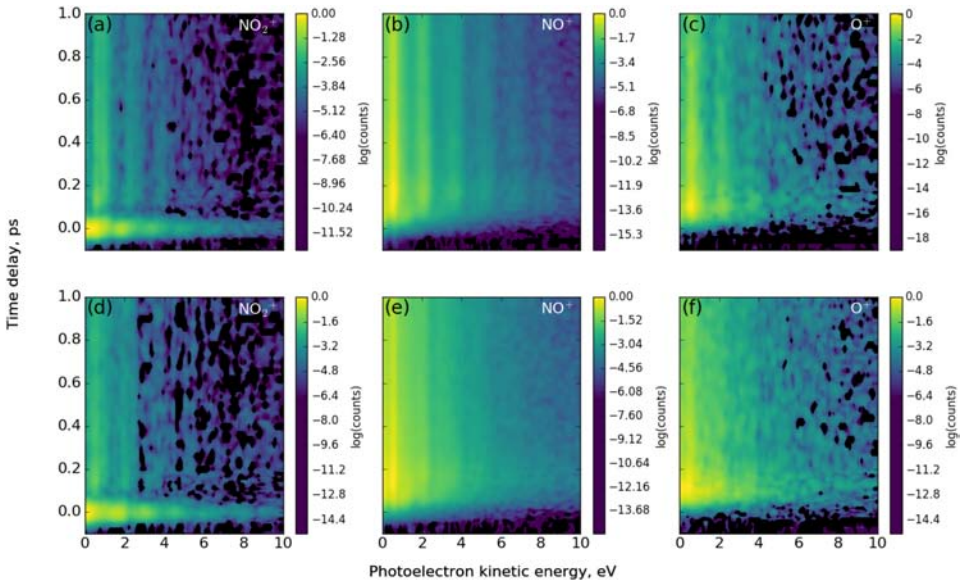

FIG. 7. TRCRATI spectra associated with NO_2^+, NO^+, and O^+ channels for two probe intensities, 3.6×10^{13} W cm^{-2} [top row, (a)–(c)] and 5.5×10^{13} W cm^{-2} [bottom row, (d)–(f)]. The spectra were recorded at a constant pump intensity of 0.8×10^{13} W cm^{-2}, and data are presented in all cases for the parallel polarization geometry.

contributions of these channels from the observed signal remains challenging.

V. DISCUSSION

A. Single photon excitation and relaxation dynamics

In these experiments, single photon excitation transfers population from the $\tilde{X}\ ^2A_1$ state to the $\tilde{A}\ ^2B_2$ state. The transition dipole moment for this transition lies along the y-axis, oxygen-oxygen axis (see Fig. 8), and excitation therefore produced a $\cos^2(\theta)$ distribution of the molecular y-axes in the laboratory frame (where θ is the angle between the molecular y-axis and the pump laser polarization). As outlined in the introduction, the excited state wavepacket moves rapidly towards the conical intersection between the $\tilde{X}\ ^2A_1$ and the $\tilde{A}\ ^2B_2$ states, with the initial motion expected to be somewhat localized along the bending coordinate, where the potential energy gradient is the greatest. The wavepacket is expected to make several passages of the conical intersection, with substantial population transfer to the ground state typically occurring in 200 fs.[41]

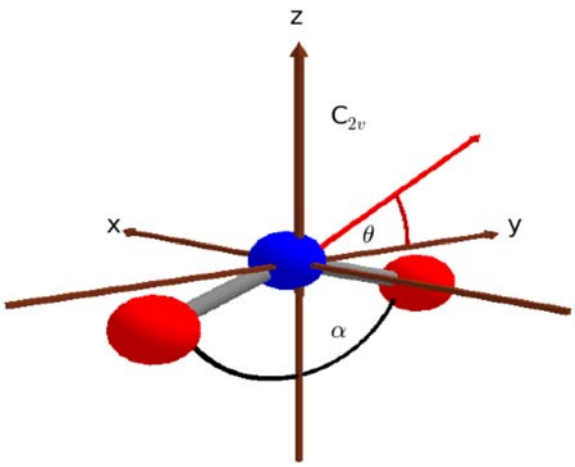

FIG. 8. Schematic diagram of the ground state equilibrium structure of NO_2 with the molecular axis labelled for C_{2v} symmetry. α is the ∠ONO bending angle, and θ is the angle between the molecular y-axis (oxygen-oxygen axis) and the pump laser polarization vector (red).

In previous experimental and theoretical work performed by Wörner *et al.*, all-electron, coupled-channel time-dependent Schrödinger equation calculations were carried out for SFI of NO_2.[8] The calculations made use of a mixed orbital/grid-based approach and calculated the SFI yield and its angular-dependence[52,53] for a series of final ionic states at a specific set of geometries within C_{2v} symmetry. For the geometries considered on the $\tilde{A}\ ^2B_2$ surface, ionization predominately correlates to the $\tilde{a}\ ^3B_2$ excited state of NO_2^+, which likely results in fragmentation to produce NO^+. Calculations performed by Hirst indicate that the $\tilde{a}\ ^3B_2$ state correlates, adiabatically, with the $NO^+(X\ ^2\Sigma^+) + O(^3P)$ dissociation limit.[54] The angular dependence for SFI to the $\tilde{a}\ ^3B_2$ state is strongly peaked along the molecular z-axis for the considered nuclear geometries. We therefore expect ionization from the $\tilde{A}\ ^2B_2$ state (and therefore NO^+ production) should be enhanced for the perpendicular polarization geometry, given that the initial axis alignment created upon photoexcitation is peaked along the y-axis.

In contrast with this expectation, increased ionization in the NO^+ channel was observed in the parallel polarization geometry, on time scales that are comparable to the expected time scale for significant population transfer (<200 fs). The prior study by Wörner *et al.* additionally reported SFI calculations from the $\tilde{X}\ ^2A_1$ state of NO_2 at two geometries corresponding to (i) the $\tilde{X}\ ^2A_1$ equilibrium geometry at an ONO bond angle (∠ONO) of 134° and (ii) the conical intersection geometry of the $\tilde{A}\ ^2B_2$ state at ∠ONO = 102°. The calculations highlight that, at bond angles in the region of 102°, the energetic ordering of the ionic $X\ ^1A_1$ and $\tilde{a}\ ^3B_2$ diabatic states switches (see Fig. 1), resulting in approximately an order of magnitude higher SFI yield for ionization correlating to the $\tilde{a}\ ^3B_2$ state at that calculated geometry. Additionally, the angle dependent SFI yield for this geometry was calculated to be strongly peaked along the molecular y-axis, in accord with the NO^+ signal polarization dependence. However, we note that the previously reported SFI calculations were

conducted at a higher intensity (1.0×10^{14} W cm^{-2}) than the measurements we report here and that the calculations were performed for a single optical cycle. These two factors mean that quantitative comparison with the previous calculation is not possible.

Consolidating these SFI calculations with (i) the expected molecular axis distribution due to the initial pump excitation, (ii) our observed enhanced ionization in the parallel geometry for the NO^+ channel at approximately 180 fs, and (iii) the wavepacket calculations, we conclude that the most likely origin of the enhanced ionization feature at 180 fs time delay is SFI from the excited molecule returning to the ground electronic state of NO_2 at bent molecular geometries. It is important to note that the feature observed in the NO^+ channel at shorter time delays (<100 fs) is associated with higher pump intensities and can be attributed to multiple pump photon dynamics in higher-lying neutral excited states in NO_2; this will be discussed in Sec. V B.

At 180 fs time delay, the NO_2^+ channel also exhibits peaks in the TRCRATI spectra. The lower energy ATI comb (0.5 + n$\hbar\omega$ eV) appears at the same electron kinetic energies as the ATI comb observed in the NO^+ TRCRATI spectra, indicating that the y-polarized SFI channel from the $\tilde{X}\ ^2A_1$ ground state surface to $\tilde{a}\ ^3B_2$ excited cationic state can also result in the formation of stable parent ions. The higher energy ATI comb (0.9 + n$\hbar\omega$ eV) can be assigned to the z-polarized ionization route, which correlates with the $X\ ^1A_1$ cationic state. This assertion is supported by the fact that the wavepacket returns to the ground state with an internal energy just below the first dissociation limit of NO_2 and, therefore, is expected to explore a large range of nuclear geometries far away from equilibrium (i.e., O atom roaming). Of particular interest is the wavepacket exploring regions on the $\tilde{X}\ ^2A_1$ surface at large ∠ONO, where the geometry approaches the linear equilibrium structure of the $X\ ^1A_1$ cationic state. Accessing near linear geometries, therefore, provides good Franck-Condon (FC) overlap for ionization as well as an effectively lower ionization potential,[54] resulting in an increased SFI rate.[8] This mechanism is further supported by the wavepacket calculations that indicate that such regions of nuclear coordinate space are accessed on similar time scales,[41,42] as well as the relatively small calculated SFI yields for ionization from the $\tilde{A}\ ^2B_2$ state away from the pump FC geometry.[8] Finally, we note that the reduced sensitivity of the NO_2^+, compared to the NO^+, ion/electron yields to the relative polarization geometry (see Fig. 3) is likely related to the participation of the multiple continua correlating to the $X\ ^1A_1$ and $\tilde{a}\ ^3B_2$ cationic states: the associated channels exhibit peaks in the angle dependent SFI yield along the y-axis and z-axis, respectively, thus averaging away sensitivity to the polarization geometry.

The $\tilde{X}\ ^2A_1$ ground state wavepacket is expected to remain somewhat localized within the bending and symmetric stretch coordinates for the first few hundred femtoseconds, meaning that ground state IVR is incomplete on the few hundred femtosecond time scale. At later times, IVR will induce the wavepacket to explore geometries at extended ON–O bond lengths (r_{ON-O}), as well as larger ∠ONO. Indeed, it is IVR and coupling into the asymmetric stretch coordinate that gives rise to the neutral dissociation process on the ground state surface, yielding NO ($X^2\Pi$) and O(^{3}P) products. This spreading of the wavepacket leads to a decay of the ionization signal associated with the $\tilde{a}\ ^3B_2$ state, due to the increase in IP away from the $\tilde{a}\ ^3B_2$ equilibrium geometry and the reduced wavepacket density in the low IP region. Conversely, an increase in SFI rate correlating to $X\ \Sigma_g^+/^1A_1/^1A'$ state of the cation is expected due to a reduction in IP in regions of coordinate space near its equilibrium geometry.[54] Ionization of the wavepacket on the neutral ground state from a range of bond angles and bond lengths is likely, therefore, to result in the formation of stable NO_2^+ as well as fragmentation to form NO^+. We speculate that the peaks observed in all ion/electron channels between 380 and 400 fs are, therefore, signatures of an increased likelihood of ionization to the ground state of the cation from the "hot" ground state of the neutral. The participation of the aforementioned multiple SFI continua, at 180 fs and 380-400 fs, is supported by the insensitivity of the latter peak (380-400 fs) to the relative laser polarization geometry, due to the fact that the two accessible ion states are reached via cross-polarized transitions (see Fig. 3). We note that the participation of the two SFI channels will result in a loss of ATI comb contrast in the NO^+ correlated spectra at 380 fs with respect to 180 fs to some degree, but under the proviso that ionization to the $\tilde{a}\ ^3B_2$ state and NO^+ production dominates, an ATI comb shift need not be observed. The dominance of the $\tilde{X}\ ^2A_1 \rightarrow \tilde{a}\ ^3B_2$ channel is substantiated by the previous SFI calculations performed by Wörner *et al.*[8] as well as the ion state literature.[54]

On longer (picosecond) time scales, the wavepacket spreading into the antisymmetric stretch coordinate results in a reduction of wavepacket density in the regions of coordinate space participating in the aforementioned channels associated with SFI to the $X\ \Sigma_g^+/^1A_1/^1A'$ and $\tilde{a}\ ^3B_2$ cationic states. This results in the decay of the NO_2^+, NO^+, and O^+ ion/electron signals. At the pump photon energy used in the experiments, a fraction of the excited molecules that return to the ground state will have an internal energy just above the NO ($X^2\ \Pi$) and O(^{3}P) dissociation limit: these molecules will dissociate on a few picosecond time scale, as discussed in detail in previous time-resolved laser induced fluorescence studies.[43] The majority of the wavepacket will however remain bound, thus the ion/electron signals do not decay to zero due to the continued but reduced possibility of ionization to the $X\ \Sigma_g^+/^1A_1/^1A'$ and $\tilde{a}\ ^3B_2$ states at intermediate bond angles and bond lengths. Furthermore, it is of note that a persistent ATI comb structure was observed in all TRCRATI spectra at long pump-probe delays (see Fig. 4), suggesting that SFI of free neutral photofragments and/or fragmentation of weakly bound NO_2^+ does not contribute to the observed ion/electron signals. If these ionization routes contributed significantly to the ionization yields, one would expect a shift of the ATI comb peak positions and/or a reduction in ATI comb contrast at longer pump-probe delays, in contradiction with what was observed. We therefore conclude that the SFI pathways observed at pump-probe delays between 100 fs and 400 fs remain open channels at these time delays. This is supported by the temporal invariance of the ATI comb structures. However, the yield of these ATI electrons decreases with time, most likely due to wavepacket spreading.

Finally, we consider the possible origins of the O^+ signal, which is undoubtedly due to accessing even higher-lying ionization continua. PEPICO spectra recorded by Eland and Karlsson show that dissociative ionization to produce $O^+(^4S_{3/2})$ in correlation with $NO(X^2\Pi_{3/2})$ can only occur at excitation energies above 16.63 eV and that the O^+ signal increases significantly above 17.4 eV.[55] We note, however, that assignment of a particular electronic configuration becomes difficult at high excitation energies due to the broad photoelectron bands associated with electron correlation and multiple electronic configurations describing the excited cation states.[54,56] The TRCRATI spectra (Fig. 4) highlight that the production of the O^+ atomic fragment is likely linked to indirect/sequential ionization. The ATI comb peak position appears at identical kinetic energies ($0.5 + n\hbar\omega$ eV) to the ATI combs present in both the NO_2^+ parent ion and NO^+ fragment correlated spectra; these channels were assigned to SFI from the $\tilde{X}\ ^2A_1$ ground state surface to the $\tilde{a}\ ^3B_2$ excited cationic state in the preceding paragraphs.

It should be noted that O^+ and N^+ fragments were previously observed in a study by Singhal *et al.*, which investigated multiphoton ionization pathways in NO_2.[57] The study employed 375 nm photons with a pulse duration of 50 fs and an estimated maximum intensity of 5×10^{13} W cm^{-2}. The authors assigned dissociative ionization of neutral NO photoproducts as the origin of the atomic ion fragments. This interpretation is, however, inconsistent with the dynamics observed at long time delays (>500 fs), as the ion/photoelectron yields associated with O^+ signal decreases a function of time, as opposed to the expected (increasing) delay dependence of a photoproduct yield. Furthermore, if dissociative ionization of free NO fragments, to produce O^+, contributed significantly, a shift of the ATI combs kinetic energy position and/or a reduction of ATI comb contrast would likely be observed at longer time delays. It is of note that, as suggested by the pump intensity study (see Fig. 5), the initial feature at 80 fs is attributed to dynamics of higher-lying neutral states in NO_2, as discussed in Sec. V B. With the single-pump photon dynamics discussed above in mind, we summarize the neutral state wavepacket evolution as follows:

$$\tilde{A}^2B_2 \overset{\text{IC}}{\underset{180\text{fs}}{\rightsquigarrow}} \tilde{X}^2A_1^{\dagger} \overset{\text{IVR}}{\underset{380\text{fs}}{\rightsquigarrow}} \tilde{X}^2A_1^{\dagger\dagger} \underset{10\text{ps}}{\rightsquigarrow} NO(X^2\Pi) + O(^3P). \quad (3)$$

In contrast to other related work,[37] we favour the above interpretation of the transient ion/photoelectron signals over a periodic vibronic wavepacket explanation. We emphasize that no signature of periodic wavepacket motion is observed in the NO_2 absorption spectrum, no clear oscillatory frequencies can be extracted from Fourier transform maps of the TRCRATI spectra and the observation that signals that were, in other studies, previously attributed to periodic vibronic motion have differing pump-intensity dependent signal strengths (see the following sub-section).

B. The role of multiphoton pump excitation and relaxation dynamics

The intense nature of ultrashort laser fields and the expected high absorption cross-sections for multiphoton pump excitations often result in complications in the interpretation

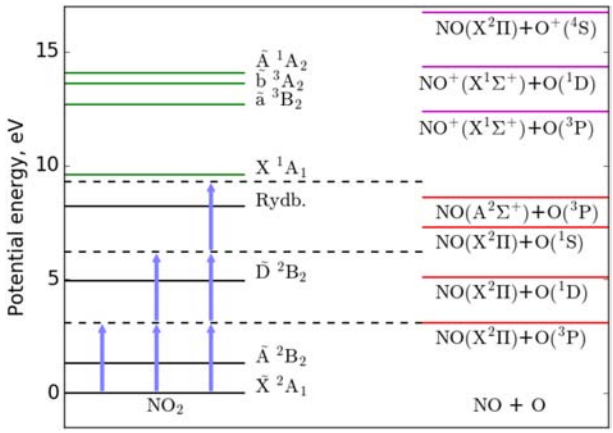

FIG. 9. Energy levels of NO_2 (black solid lines) and NO_2^+ (green solid lines) as well as various neutral dissociation thresholds and photofragmentation channels (black dashed lines), indicated are the possible multiphoton excitation pathways to the $\tilde{D}\ ^2B_2$ state and the Rydberg manifold. The 399 nm pump photon is represented as a blue arrow and the neutral (red solid lines) and ionic (magenta solid lines) states of the NO and O fragments are shown to the right of the figure.

of results in many femtosecond time-resolved studies.[36,38,39,46] This is particularly true if the experimental observable is not directly sensitive to the number of pump photons absorbed. At the pump photon energy employed in the experiments, two- and three-photon excitations could occur to the higher-lying (neutral) $\tilde{D}\ ^2B_2$ excited state and the Rydberg manifold, respectively (see Fig. 9). Both of these processes would be resonantly enhanced by the one-photon resonance with the $\tilde{A}\ ^2B_2$ state. Signatures of these multiphoton excitation pathways were directly observed in our higher pump intensity dependent data, for both the NO^+ and O^+ channels at short delay times (<100 fs). This has important consequences for the interpretation of all pump-probe experiments on NO_2 using strong laser fields.

We first consider the $\tilde{D}\ ^2B_2$ state; although accessing the state directly via two-photon absorption is dipole allowed, additionally, two resonantly enhanced excitation pathways are possible. Excitation to the $\tilde{D}\ ^2B_2$ state can occur by using $\tilde{A}\ ^2B_2$ as a doorway state and subsequent single-photon excitation to the $\tilde{D}\ ^2B_2$ state is a z-polarized dipole allowed transition,

$$\tilde{X}^2A_1 \overset{h\nu}{\underset{y}{\longrightarrow}} \tilde{A}^2B_2 \overset{h\nu}{\underset{z}{\longrightarrow}} \tilde{D}^2B_2. \quad (4)$$

A second excitation route is possible due to the wavepacket being able to make the first pass through the conical intersection within the pump pulse duration. Therefore, the initially populated state could dynamically acquire considerable $\tilde{X}\ ^2A_1$ character within the pump pulse duration, allowing the $\tilde{D}\ ^2B_2$ state to be accessed through the absorption of a second 399 nm photon,

$$\tilde{X}^2A_1 \overset{h\nu}{\underset{y}{\longrightarrow}} \tilde{A}^2B_2 \overset{\text{IC}}{\rightsquigarrow} \tilde{X}^2A_1^{\dagger} \overset{h\nu}{\underset{y}{\longrightarrow}} \tilde{D}^2B_2. \quad (5)$$

The $\tilde{D}\ ^2B_2$ state is expected to predissociate within 100 fs[58] via one of two dissociation thresholds, producing either $NO(^2\Pi) + O(^1D)$ (the second dissociation limit at 5.08 eV) or $NO(^2\Pi) + O(^3P)$ (the first dissociation limit at 3.11 eV, see Fig. 9).[27,59] The production of both NO^+ and O^+ due to ionization of free neutral photofragments giving rise to the features observed

at <100 fs can be ruled out, since these ion signals rapidly decay after reaching a maximum. Since free neutral dissociation products cannot vanish once formed, ionization of neutral photofragments would yield a signal that would increase asymptotically and then effectively remain constant out to very long time delays,[26,27,40] in contrast to what was observed in our data.

We expect that the primary ionization routes from the $\tilde{D}\,^2B_2$ state will result in the population of unstable electronically and vibrationally excited states in NO_2^+, likely the $\tilde{b}\,^3A_2$ and $\tilde{A}\,^1A_2$ states, that are expected to fragment to produce NO^+ ions.[29] The well structured ATI comb observed at later time delays in the high pump intensity fragment channel data sets [see Figs. 6(d)–6(f)] is notably absent at pump-probe delays <100 fs. The absence of a clear ATI comb points towards the participation of additional ionization channels and correlation to an increased number of final ionic states, thereby supporting the proposed mechanism.[63–66]

A second possibility is that the origin of the multiphoton pump dynamics is via three-photon absorption to the Rydberg manifold, which would be resonantly enhanced at both single and potentially the two-photon level. Similar to the discussion of two-pump-photon excitation, it is possible that, following single-photon excitation to the $\tilde{A}\,^2B_2$ manifold, subsequent excitation occurs from vibrationally excited levels on the $\tilde{X}\,^2A_1$ state following passage through the conical intersection. Accessing the $\tilde{X}\,^2A_1$ state results in many nuclear geometries being sampled, along the bending coordinate and, therefore, provides good FC overlap with the linear geometry Rydberg series: these typically have poor FC overlap for direct single-photon transitions from the $\tilde{X}\,^2A_1$ state.[60–62] At excitation energies corresponding to three-photons at 399 nm, multiple dissociation thresholds and non-adiabatic couplings are expected to play a role in the ensuing fragmentation dynamics.[40] However, similarly to the case of two-pump-photon excitation, we can rule out that the signal originates from ionization of free neutral photofragments produced through neutral dissociation. Direct SFI of Rydberg states should result in the well-known Freeman resonances[14] due to the low binding energies of these states. As is well-known, due to their low IP, such features in an ATI comb cannot persist out to higher orders of the comb. Our data show some tentative evidence for this: in addition to the fragment, NO^+ and O^+, channels at 80 fs not showing a well structured ATI comb at higher pump intensities, there is a narrow feature observed at around 1 eV, which exhibits only a single peak at higher photoelectron kinetic energies [Figs. 6(d) and 6(e)]. This is consistent with the 1 eV feature being due to a Freeman resonance—the SFI of higher-lying Rydberg states.

Finally, we turn our attention to the polarization geometry dependence observed in features correlated with multiphoton pump excitation in the NO^+ and O^+ channels (see Fig. 5). As discussed in Sec. V A, the transition dipole moment associated with single-photon-pump excitation lies along the molecular y axis. The transition dipole moment associated with the absorption of a second 399 nm photon can potentially lie along either the z-axis [see Eq. (4)] or y-axis [see Eq. (5)] depending upon if the population undergoing a second pump photon excitation possess $\tilde{A}\,^2B_2$ or $\tilde{X}\,^2A_1$ character, respectively. Therefore, a sequential excitation process will result in either a complex molecular axis distribution, if the transition dipole moments for each of the single-photon excitations lie along different molecular axes, or a sharpening of the initial lab frame molecular axis distribution, producing a $\cos^4(\theta)$ distribution of the y molecular axis. In the case of three-photon excitation to the Rydberg manifold, population of a particular Rydberg state will primarily be selected based upon the electronic character of the state. However, at excitation energies corresponding to two- or three-photons at 399 nm, a large number of non-adiabatic couplings are expected to play a role in the ensuing dynamics.[40] The sensitivity of the polarization geometry and the observed enhancement of the NO^+ and O^+ signals could therefore reflect a change in electronic character rather than originating from alignment created by the pump laser photoexcitation.

Given the available information in the current experimental data, disentangling of the multiphoton contributions arising from two- or three-pump-photon excitation remains challenging, particularly as the ATI comb structure in the TRCRATI spectrum loses contrast in the higher pump intensity data sets. The time scale of the features observed in the fragment channels is somewhat indicative of the predissociating $\tilde{D}\,^2B_2$ state but the sharp spectral features at around 1 eV in the TRCRATI spectrum correlated with NO^+ could be a signature of ionization of a Rydberg state. The origin of the O^+ signal is also hard to assign but we speculate that a similar interpretation to Sec. V A may be appropriate, where the increase in signal originates from ionization of molecules at extended r_{ON-O}. Although the fragment channels show sensitivity to the relative polarization geometry, identifying the origin of this is difficult without SFI calculations from higher-lying excited states in NO_2. Both the two- and three-pump-photon excitation processes have been identified previously in both femtosecond time-resolved imaging and coincidence imaging experiments[36,38,39] but a more detailed experimental study would be required to examine this in the SFI case.

VI. CONCLUSION

We have reported a femtosecond time-resolved study utilising SFI and photoelectron-photoion coincidence spectroscopy to investigate excited state wavepacket dynamics in NO_2. Channel-resolved above-threshold ionization (CRATI) experiments reveal modulations in both the total photoelectron and photoion yields for all channels considered. We have shown that the origin of these modulations is due to an incoherent combination of single and multiphoton pump excitations and their subsequent dynamics, as opposed to the previously reported periodic vibronic wavepacket motion. The contributions of non-adiabatic coupling rapidly re-populating the ground state were recognised through comparing the relative polarization geometry studies with recently published SFI and wavepacket calculations. In addition, the effects of two/three-pump-photon excitation dynamics, at short time delays, <100 fs, were identified through the pump intensity investigation and the detection of fragment photoelectrons and ions in coincidence. The longer time scale dynamics are

tentatively attributed to signatures of ionization of the "hot" ground state wavepacket, due to an increase in SFI rate to the cationic ground state.

More generally, these results highlight the complexity of tracking non-adiabatic dynamics in polyatomic molecules using SFI, due to the presence of multiple electronic continua accessed during ionization. The experimental results present a situation where even a reasonably differential measurement, such as exploiting photoelectron and fragment coincidences, remains challenging for determining the role of multielectron effects. A future extension of this work to investigate fragment kinetic energy release would be of interest to help further disentangle the role of these effects and verify our current assignments. Additionally, a more complete set of SFI calculations that take into account asymmetric stretch geometries would provide a more detailed comparison with the current experimental results and conclusions. Future studies to investigate the effect of pump wavelength on the long-lived picosecond decay would also provide more insight into the dissociation dynamics.

ACKNOWLEDGMENTS

R.F. is grateful to the Engineering and Physical Sciences Research Council (EPSRC) for a research studentship. A.S. thanks the NSERC Discovery Grant program for financial support. We are grateful to Varun Suresh Makhija, Michael Spanner, Paul Hockett, and Rune Lausten for useful discussions.

[1] A. E. Boguslavskiy, J. Mikosch, A. Gijsbertsen, M. Spanner, S. Patchkovskii, N. Gador, M. J. J. Vrakking, and A. Stolow, Science **335**, 1336 (2012).
[2] J. Mikosch, A. E. Boguslavskiy, I. Wilkinson, M. Spanner, S. Patchkovskii, and A. Stolow, Phys. Rev. Lett. **110**, 023004 (2013).
[3] S. Baker, J. S. Robinson, C. A. Haworth, H. Teng, R. A. Smith, C. C. Chirila, M. Lein, J. W. G. Tisch, and J. P. Marangos, Science **312**, 424 (2006).
[4] W. Li, X. Zhou, R. Lock, S. Patchkovskii, A. Stolow, H. C. Kapteyn, and M. M. Murnane, Science **322**, 1207 (2008).
[5] O. Smirnova, Y. Mairesse, S. Patchkovskii, N. Dudovich, D. M. Villeneuve, P. B. Corkum, and M. Y. Ivanov, Nature **460**, 972 (2009).
[6] H. J. Wörner, J. B. Bertrand, D. V. Kartashov, P. B. Corkum, and D. M. Villeneuve, Nature **466**, 604 (2010).
[7] S. Matsika, M. Spanner, M. Kotur, and T. C. Weinacht, J. Phys. Chem. A **117**, 12796 (2013).
[8] H. J. Wörner, J. B. Bertrand, B. Fabre, J. Higuet, H. Ruf, A. Dubrouil, S. Patchkovskii, M. Spanner, Y. Mairesse, V. Blanchet, E. Mével, E. Constant, P. B. Corkum, and D. M. Villeneuve, Science **334**, 208 (2011).
[9] H. Ruf, C. Handschin, A. Ferré, N. Thiré, J. B. Bertrand, L. Bonnet, R. Cireasa, E. Constant, P. B. Corkum, D. Descamps, B. Fabre, P. Larregaray, E. Mével, S. Petit, B. Pons, D. Staedter, H. J. Wörner, D. M. Villeneuve, Y. Mairesse, P. Halvick, and V. Blanchet, J. Chem. Phys. **137**, 224303 (2012).
[10] P. M. Kraus, Y. Arasaki, J. B. Bertrand, S. Patchkovskii, P. B. Corkum, D. M. Villeneuve, K. Takatsuka, and H. J. Wörner, Phys. Rev. A **85**, 043409 (2012).
[11] A. Tehlar and H. J. Wörner, Mol. Phys. **111**, 2057 (2013).
[12] P. B. Corkum, Phys. Rev. Lett. **71**, 1994 (1993).
[13] M. Lewenstein, P. Balcou, M. Y. Ivanov, A. LHuillier, and P. B. Corkum, Phys. Rev. A **49**, 2117 (1994).
[14] R. R. Freeman, P. H. Bucksbaum, H. Milchberg, S. Darack, D. Schumacher, and M. E. Geusic, Phys. Rev. Lett. **59**, 1092 (1987).
[15] B. K. McFarland, J. P. Farrell, P. H. Bucksbaum, and M. Gühr, Science **322**, 1232 (2008).
[16] H. Akagi, T. Otobe, A. Staudte, A. Shiner, F. Turner, R. Dörner, D. M. Villeneuve, and P. B. Corkum, Science **325**, 1364 (2009).
[17] R. Torres, T. Siegel, L. Brugnera, I. Procino, J. G. Underwood, C. Altucci, R. Velotta, E. Springate, C. Froud, I. C. E. Turcu, S. Patchkovskii, M. Y. Ivanov, O. Smirnova, and J. P. Marangos, Phys. Rev. A **81**, 051802 (2010).
[18] M. Spanner, J. Mikosch, A. E. Boguslavskiy, M. M. Murnane, A. Stolow, and S. Patchkovskii, Phys. Rev. A **85**, 033426 (2012).
[19] A. Ferré, A. E. Boguslavskiy, M. Dagan, V. Blanchet, B. D. Bruner, F. Burgy, A. Camper, D. Descamps, B. Fabre, N. Fedorov, J. Gaudin, G. Geoffroy, J. Mikosch, S. Patchkovskii, S. Petit, T. Ruchon, H. Soifer, D. Staedter, I. Wilkinson, A. Stolow, N. Dudovich, and Y. Mairesse, Nat. Commun. **6**, 5952 (2015).
[20] Q. Ji, S. Cui, X. You, X. Gong, Q. Song, K. Lin, H. Pan, J. Ding, H. Zeng, F. He, and J. Wu, Phys. Rev. A **92**, 043401 (2015).
[21] *VUV and Soft X-Ray Photoionization*, edited by U. Becker and D. A. Shirley (Springer US, Boston, MA, 1996).
[22] M. Lezius, V. Blanchet, D. M. Rayner, D. M. Villeneuve, A. Stolow, and M. Y. Ivanov, Phys. Rev. Lett. **86**, 51 (2001).
[23] M. Lezius, V. Blanchet, M. Y. Ivanov, and A. Stolow, J. Chem. Phys. **117**, 1575 (2002).
[24] R. E. Smalley, J. Chem. Phys. **61**, 4363 (1974).
[25] H. Zacharias, J. Chem. Phys. **74**, 218 (1981).
[26] L. Bigio and E. R. Grant, AIP Conf. Proc. **146**, 501 (1986).
[27] L. Bigio and E. R. Grant, J. Chem. Phys. **87**, 360 (1987).
[28] S. A. Reid and H. Reisler, J. Phys. Chem. **100**, 474 (1996).
[29] G. K. Jarvis, Y. Song, C. Y. Ng, and E. R. Grant, J. Chem. Phys. **111**, 9568 (1999).
[30] I. Bezel, P. Ionov, and C. Wittig, J. Chem. Phys. **111**, 9267 (1999).
[31] I. Bezel, D. Stolyarov, and C. Wittig, J. Phys. Chem. A **103**, 10268 (1999).
[32] M. Brouard, R. Cireasa, A. P. Clark, T. J. Preston, and C. Vallance, J. Chem. Phys. **124**, 64309 (2006).
[33] R. B. Lopez-Martens, T. W. Schmidt, and G. Roberts, J. Chem. Phys. **111**, 7183 (1999).
[34] A. T. J. B. Eppink, B. J. Whitaker, E. Gloaguen, B. Soep, A. M. Coroiu, and D. H. Parker, J. Chem. Phys. **121**, 7776 (2004).
[35] N. T. Form, B. J. Whitaker, L. Poisson, and B. Soep, Phys. Chem. Chem. Phys. **8**, 2925 (2006).
[36] A. Vredenborg, W. G. Roeterdink, and M. H. M. Janssen, J. Chem. Phys. **128**, 204311 (2008).
[37] B. Liu, J. Zhu, B. Wang, Y. Wang, and L. Wang, J. Phys. Chem. A **113**, 13839 (2009).
[38] D. Irimia, I. D. Petsalakis, G. Theodorakopoulos, and M. H. M. Janssen, J. Phys. Chem. A **114**, 3157 (2010).
[39] J. B. Hamard, R. Cireasa, B. Chatel, V. Blanchet, and B. J. Whitaker, J. Phys. Chem. A **114**, 3167 (2010).
[40] I. Wilkinson and B. J. Whitaker, Annu. Rep. Sect. C: Phys. Chem. **106**, 274 (2010).
[41] Y. Arasaki, K. Takatsuka, K. Wang, and V. McKoy, J. Chem. Phys. **132**, 124307 (2010).
[42] U. Manthe and H. Koppel, J. Chem. Phys. **93**, 1658 (1990).
[43] S. I. Ionov, G. A. Brucker, C. Jaques, Y. Chen, and C. Wittig, J. Chem. Phys. **99**, 3420 (1993).
[44] A. G. Suits, Acc. Chem. Res. **41**, 873 (2008).
[45] M. Sanrey and M. Joyeux, J. Chem. Phys. **126**, 074301 (2007).
[46] I. Wilkinson, A. E. Boguslavskiy, J. Mikosch, J. B. Bertrand, H. J. Wörner, D. M. Villeneuve, M. Spanner, S. Patchkovskii, and A. Stolow, J. Chem. Phys. **140**, 204301 (2014).
[47] H. K. Roscoe and A. K. Hind, J. Atmos. Chem. **16**, 257 (1993).
[48] T. Tsuboi, E. Y. Xu, Y. K. Bae, and K. T. Gillen, Rev. Sci. Instrum. **59**, 1357 (1988).
[49] W. C. Wiley and I. H. McLaren, Rev. Sci. Instrum. **26**, 1150 (1955).
[50] L. J. Frasinski, K. Codling, and P. A. Hatherly, Science **246**, 1029 (1989).
[51] L. J. Frasinski, M. Stankiewicz, P. A. Hatherly, G. M. Cross, K. Codling, A. J. Langley, and W. Shaikh, Phys. Rev. A **46**, R6789 (1992).
[52] M. Spanner and S. Patchkovskii, Phys. Rev. A **80**, 063411 (2009).
[53] M. Spanner and S. Patchkovskii, Chem. Phys. **414**, 10 (2013).
[54] D. M. Hirst, J. Chem. Phys. **115**, 9320 (2001).
[55] J. H. D. Eland and L. Karlsson, Chem. Phys. **237**, 139 (1998).
[56] J. Schirmer, L. Cederbaum, and W. Von Niessen, Chem. Phys. **56**, 285 (1981).

[57]R. P. Singhal, H. S. Kilic, K. W. D. Ledingham, C. Kosmidis, T. McCanny, A. J. Langley, and W. Shaikh, Chem. Phys. Lett. **253**, 81 (1996).
[58]K. Tsuji, M. Ikeda, J. Awamura, A. Kawai, and K. Shibuya, Chem. Phys. Lett. **374**, 601 (2003).
[59]L. Bigio and E. R. Grant, J. Chem. Phys. **87**, 5589 (1987).
[60]R. S. Tapper, R. L. Whetten, G. S. Ezra, and E. R. Grant, J. Phys. Chem. **88**, 1273 (1984).
[61]M. B. Knickelbein, K. S. Haber, L. Bigio, and E. R. Grant, Chem. Phys. Lett. **131**, 51 (1986).
[62]K. S. Haber, J. W. Zwanziger, F. X. Campos, R. T. Wiedmann, and E. R. Grant, Chem. Phys. Lett. **144**, 58 (1988).
[63]J. W. Au and C. E. Brion, Chem. Phys. **218**, 109 (1997).
[64]C. F. Jackels and E. R. Davidson, J. Chem. Phys. **65**, 2941 (1976).
[65]P. Kruit and F. H. Read, J. Phys. E **16**, 313 (1983).
[66]R. Schinke, J. Chem. Phys. **129**, 124303 (2008).